

DEMONSTRATION OF A GOES-R SATELLITE CONVECTIVE TOOLKIT TO “BRIDGE THE GAP” BETWEEN SEVERE WEATHER WATCHES AND WARNINGS

An Example from the 20 May 2013
Moore, Oklahoma, Tornado Outbreak

BY CHAD M. GRAVELLE, JOHN R. MECIKALSKI, WILLIAM E. LINE, KRISTOPHER M. BEDKA, RALPH A. PETERSEN, JUSTIN M. SIEGLAFF, GEOFFREY T. STANO, AND STEVEN J. GOODMAN

Integrating GOES-R convective products into the forecaster decision-making process can provide information on preconvective conditions, short-term environmental changes with respect to the occurrence and evolution of new convective storms, and severe weather signatures.

The next generation of the Geostationary Operational Environmental Satellite (GOES) series, GOES-R, is planned to launch in early 2016 and will offer improved spacecraft and instrument technology to provide more accurate, detailed,

and timely detection of high-impact environmental phenomena. The cornerstone of GOES-R is the Advanced Baseline Imager (ABI; Schmit et al. 2005), a 16-channel imager with 2 visible channels, 4 near-infrared channels, and 10 infrared (IR) channels.

AFFILIATIONS: GRAVELLE—NOAA/NWS/Operations Proving Ground, Kansas City, Missouri, and Cooperative Institute for Meteorological Satellite Studies, University of Wisconsin–Madison, Madison, Wisconsin; MECIKALSKI—Atmospheric Science Department, University of Alabama in Huntsville, Huntsville, Alabama; LINE—NOAA/NWS/Storm Prediction Center, and Cooperative Institute for Mesoscale Meteorological Studies, University of Oklahoma, Norman, Oklahoma; BEDKA—Science Directorate, NASA Langley Research Center, Hampton, Virginia; PETERSEN AND SIEGLAFF—Cooperative Institute for Meteorological Satellite Studies, University of Wisconsin–Madison, Madison, Wisconsin; STANO—NASA Short-Term Prediction Research and Transition Center, and ENSCO, Inc.,

Huntsville, Alabama; GOODMAN—GOES-R Program Office, NASA Goddard Space Flight Center, and NOAA/National Environmental Satellite, Data, and Information Service, Greenbelt, Maryland

CORRESPONDING AUTHOR: Chad Gravelle, NOAA/NWS/Operations Proving Ground, 7220 N.W. 101st Terr., Kansas City, MO 64153
E-mail: chad.gravelle@noaa.gov

The abstract for this article can be found in this issue, following the table of contents.

DOI:10.1175/BAMS-D-14-00054.1

In final form 19 February 2015
©2016 American Meteorological Society

When compared to the current GOES imager, the ABI will provide 3 times more spectral information, 4 times the spatial resolution, and 5 times the temporal resolution. Additional advancements over current GOES capabilities include continuous total lightning detection and mapping of in-cloud and cloud-to-ground flashes from the Geostationary Lightning Mapper (GLM; Goodman et al. 2013) and increased dynamic range, resolution, and sensitivity imaging of solar activity with the Solar Ultraviolet Imager.

To simplify analyzing GOES-R data for users, the GOES-R program will produce a baseline set (i.e., those that are funded for operational implementation as part of the ground segment base contract) of atmosphere, land, ocean, solar, and space weather products that will have a wide range of uses in areas such as severe weather, heavy precipitation and flash flooding, energy, transportation, and commerce. In addition, new and enhanced applications will be possible as “future capabilities” for the GOES-R series (Goodman et al. 2012). The National Oceanic and Atmospheric Administration (NOAA) Algorithm Working Group, in conjunction with the GOES-R Risk Reduction Research (GOES-R3) science program, oversees the development, testing, demonstration, and validation of the algorithms that create these products. The GOES-R3 program enables scientists to develop “fused” algorithms that make use of data from multiple platforms, including, but not limited to, satellite, radar, numerical weather prediction model output, and surface observations.

The GOES-R Proving Ground was established in 2008 with the goal of preparing the user communities for GOES-R data (Goodman et al. 2012). The research-to-operations effort provides a variety of users, NOAA and non-NOAA, preoperational (i.e., demonstration) products that utilize current GOES data, higher-spatial-resolution data provided by operational and research satellites, ground-based observations, and/or model-derived synthetic satellite imagery. Users at National Weather Service (NWS) weather forecast offices (WFOs), the National Centers for Environmental Prediction, and a variety of NOAA test beds evaluate the utility of these demonstration products in the forecast and warning processes. The feedback provided by user evaluations of GOES-R products, decision aids, and training resources allows the algorithm developers to refine and enhance these applications (Ralph et al. 2013). The following section describes four GOES-R future capability convective storm products—0–9-h NearCast model, 0–1-h convective initiation probabilities, convective cloud-top cooling, and

overshooting top detection—and one GOES-R baseline product—the pseudo-Geostationary Lightning Mapper total lightning tendency diagnostic. These convective products were developed to aid in diagnosing characteristics of the preconvective environment and deep, moist convection (hereafter called convection).

GOES-R CONVECTIVE PRODUCTS. *NearCast*

model. The NearCast model uses a Lagrangian approach to project full-resolution 10-km GOES sounder moisture and temperature retrievals forward in time and space (Petersen et al. 2010, 2011, 2013). Wind and height data interpolated from the most recent Global Forecast System (GFS; Caplan et al. 1997) forecast cycle are used to initialize the trajectories at multiple vertical levels and to provide the height tendency information needed to compute the parcel accelerations. The Lagrangian approach allows the use of 10-min time steps, enabling forecast products to be available 5 min after the hourly GOES retrievals are processed. The irregularly spaced trajectory data from each NearCast cycle are combined with NearCast forecasts made during the previous 9 h and transferred onto regularly spaced grids for display at half-hour intervals. The merger of trajectories based on current and past observations reduces data voids caused by the presence of clouds in the most recent GOES sounder IR observations, further increasing the utility of every GOES sounding. Since the GOES retrievals used during the trajectory computations are not smoothed, observed gradients, maxima, and minima that often provide the focus for subsequent convective initiation are preserved in the analyses and 1–9-h forecast products. Equivalent potential temperature (θ_e) and layer precipitable water (PW) are obtained from the GOES retrievals in two vertically independent layers, as defined by the GOES channel-weighting functions centered near 780 and 500 hPa (Hannon et al. 1996). Deep-layer θ_e differences are then computed from the gridded forecast parameters to provide an objective means of identifying where convective instability is expected to change in the next 9 h. While the model originally computed trajectories along constant pressure surfaces, an isentropic version has been developed that, more appropriately, projects the observations through space along constant potential temperature surfaces (Line 2013). Although GOES-R will not carry the originally planned hyperspectral IR sounder, the NearCast model will utilize vertical profiles of ABI multichannel moisture observations (Schmit et al. 2008) in the GOES-R era.

The NearCast system was developed to increase forecast use of GOES sounder products (Schmit et al. 2008) and to address several key forecast issues, among them the poor accuracy of traditional short-term numerical weather prediction (NWP) precipitation and hazardous convective weather forecasts, especially during the warm season (Petersen et al. 2013). Forecasts from the NearCast model have been shown to be useful in identifying where and when convection is more likely or less likely to develop up to 9 h into the future (Petersen et al. 2011). Additionally, the total moisture content of the isentropic-layer parameter has proven skillful in highlighting areas where heavy rainfall may be more likely to occur (Line 2013). Forecaster feedback from various NOAA test beds and demonstrations has shown that NearCast products enhance and complement other forecast and analysis tools, most notably those that identify the presence of forcing mechanisms for convection (Terborg and Gravelle 2012; Line 2014). This synergy includes products such as GOES-R convective initiation and convective cloud-top cooling, as the thermodynamic fields in the NearCast model can increase or decrease confidence in current and future convective storm development that is highlighted by other algorithms and model products.

Convective initiation. It is well known that the GOES platform is ideal for providing early indications of the potential initiation of thunderstorms (e.g., Purdom 1976, 1982). To exploit this GOES capability, the GOES-R convective initiation (CI; Walker et al. 2012) product was developed from a cloud-object-tracking, geostationary satellite-based, NWP-model-fused probabilistic algorithm that identifies which cumulus clouds are more likely to produce heavy rainfall or a thunderstorm in the next hour. The Walker et al. (2012) approach uses the same geostationary satellite IR interest fields as Mecikalski and Bedka (2006) and Mecikalski et al. (2008) within a logistic regression procedure (Hosmer and Lemeshow 1989) to produce a 0%–100% probability that a given cumulus cloud object will develop into a ≥ 35 -dBZ-intensity radar echo at -10°C altitude. This definition of CI (i.e., a ≥ 35 -dBZ-intensity radar echo at -10°C altitude) is consistent with many early radar-based studies (Browning and Atlas 1965; Wilson and Schreiber 1986; Wilson et al. 1992; Wilson and Mueller 1993; Mueller et al. 2003; Roberts and Rutledge 2003). The Mecikalski and Bedka (2006) and Walker et al. (2012) approach, using a cloud-typing algorithm designed to identify convective clouds of various types (Berendes et al. 2008), focuses on the physical aspects of cumulus

clouds that can be readily observed by geostationary satellites (e.g., cloud-top height, cloud growth rates, cloud-top glaciation, and updraft persistence and width). Although an improvement over the previous version of the algorithm, the Walker et al. (2012) method did not include direct knowledge about the atmospheric environment in which clouds grow. For example, if a developing cumulus cloud shows very strong signals of vertical growth observed in satellite observations, the GOES-R CI algorithm is designed to output a high probability of CI. If the rapid vertical cloud growth is occurring beneath a strong midlevel capping inversion, this output may be misleading because the likelihood of continued development and CI is low. Therefore, Mecikalski et al. (2015) provided a significant update to the CI algorithm by introducing the use of 15 fields from the 13-km grid length NOAA Rapid Update (RAP) model, which bring to the logistic regression equations information on the mesoscale environment in which a cumulus cloud may develop. Rapid Refresh model information currently in the GOES-R CI algorithm includes surface and most unstable convective available potential energy, convective inhibition, best lifted index, lifted condensation level, convective condensation level, level of free convection, bulk and low-level wind shear, and freezing-level height. The inclusion of additional NWP predictor fields, cloud object information, and derived cloud properties from GOES (e.g., Heidinger and Pavolonis 2009; Walther and Heidinger 2012) is being investigated to improve CI predictions at night and within areas of thin cirrus clouds (Mecikalski et al. 2011, 2013) and to identify more significant events.

From the mesoanalyst or warning forecaster perspective, one of the challenges involves determining where CI is more likely to occur within an area of cumulus clouds. The GOES-R CI algorithm provides forecasters with the ability to identify where and when convective storm development is possible or likely to occur. Furthermore, since the CI algorithm focuses on many convective cloud elements, it can be used to monitor the gradual weakening of a capping inversion or the growth of cumulus clouds along boundaries by monitoring trends in the probabilistic output. This information increases our situational awareness of an unfolding convective storm event, which in turn can allow forecasters to update short-term forecasts and provide improved support to interested NWS partners (e.g., when monitoring convection for outdoor events). Currently, GOES-R CI lead times at 50% or greater probability are generally between 30 and 50 min, shorter in environments that are more

unstable and longer when cumulus cloud growth is gradual (Mecikalski et al. 2015). Since 2010, the GOES-R CI product has been evaluated at more than 10 NWS WFOs, at the Hazardous Weather Testbed (HWT; Clark et al. 2012; Ralph et al. 2013), and at the Aviation Weather Testbed (AWT; Levit et al. 2011; Ralph et al. 2013). These evaluations have provided invaluable feedback that has led to algorithm improvements and effective practices for integrating the product into NWS operations (e.g., Line 2014). NWS forecasters typically integrate the product with other guidance as a means of assessing the short-term likelihood of convection.

Cloud-top cooling detection. The convective cloud-top cooling (CTC) algorithm was designed to quantitatively diagnose the strength of vertical convective cloud growth as observed by geostationary weather satellites (Sieglauff et al. 2011, 2014). Given the small spatial and short time scales of rapidly developing deep convection, the high spatial and temporal resolutions (1–4 km and 5–15 min, respectively) of NOAA’s current suite of GOES satellites are well suited to monitor the potential for high-impact meteorological phenomena. The algorithm uses a computationally efficient boxed-averaged approach to determine infrared window (IRW) brightness temperature (BT) cooling observed between consecutive GOES imager scans of vertically developing convective clouds. The evolution of the algorithm was shaped largely by iterative feedback between NOAA researchers and operational forecasters at the NWS. For example, forecasters consistently suggested that improvements to the CTC algorithm’s performance be made in regions of thin cirrus clouds and that the developers should determine relationships between CTC rates and Next Generation Weather Radar (NEXRAD) storm attributes. To solve the thin cirrus problem, algorithm developers incorporated temporal trends of GOES-derived visible optical depth (Walther and Heidinger 2012) between two consecutive GOES imager scans to permit diagnosis of cloud-top cooling rates even in regions of thin cirrus clouds during daytime hours (Sieglauff et al. 2014). Using the refined algorithm, analysis indicated a correlation between CTC rate and future NEXRAD storm intensity [using composite reflectivity, reflectivity at the -10°C isotherm, vertically integrated liquid, and maximum expected size of hail (MESH)] as the probability of detection was 0.83 and 0.71 for ≥ 1.00 -in. MESH and 60 dBZ at the -10°C isotherm, respectively, for all CTC detections.

The updated convective CTC algorithm output is designed to help forecasters address two forecast problems: 1) diagnose where robust convective clouds are developing and 2) relate the satellite-inferred cloud growth intensity to future NEXRAD-observed storm intensity. In the test bed environment at the HWT, forecasters used CTC rates with the MESH values to improve situational awareness. This allowed forecasters to issue experimental severe thunderstorm warnings, generally one to four NEXRAD volume scans (~ 5 – 20 min) earlier than with radar alone. The successes demonstrated at the HWT and AWT led to the experimental ingestion of CTC rates at select NWS WFOs and the Storm Prediction Center (SPC), where CTC rates have been mentioned in many mesoscale discussion products by the SPC and a few area forecast discussion updates by WFOs. Using the CTC rate output with the NearCast and CI products, the forecaster’s situational awareness is increasingly heightened as the CTC algorithm identifies which of the developing storms will likely intensify and produce hazards within the next 60 min.

Pseudo-Geostationary Lightning Mapper flash extent density. Ground-based total lightning observations (i.e., both intracloud and cloud-to-ground lightning) are provided by regional lightning mapping arrays (LMAs; Rison et al. 1999; Thomas et al. 2004) to simulate the capabilities of the GLM. An LMA network detects very-high-frequency (VHF) radiation sources as a developing lightning flash emits electromagnetic radiation across a broad range of frequencies (Maggio et al. 2005) and maps them using a time-of-arrival technique (Proctor 1971, 1981; Lennon 1975; Maier et al. 1995). The VHF source detections represent stepped leader formation of lightning during the early stage of a lightning flash before the visible return stroke, although VHF sources can also be observed after a return stroke. The VHF sources are then recombined into flashes using flash reconstruction algorithms (McCaul et al. 2005). Although the ground-based LMAs and the GLM detect different aspects of the lightning flash (VHF vs optical detection), the observations from the LMAs provide the total lightning measurement concepts and use case examples to train forecasters to become better prepared for the GLM. To generate the pseudo-Geostationary Lightning Mapper (pGLM) flash extent density product, the raw VHF sources from the ground-based LMAs are used and recombined via a flash creation algorithm (McCaul et al. 2009). Finally, the flashes are mapped onto an 8 km \times 8 km grid to simulate the resolution of the GLM,

and the final pGLM flash extent density product counts the number of flashes that traverse each grid box summed over 2-min intervals.

Once generated and displayed, the pGLM flash extent density product demonstrates an important capability of total lightning: the ability to assess the flash-rate tendency relationship between total lightning and the strength of a thunderstorm's updraft at a high temporal resolution (compared to radar volume scan updates). Increases (decreases) in total lightning indicate a strengthening (weakening) updraft (Lhermitte and Krehbiel 1979; Tessendorf et al. 2005; Kuhlman et al. 2006; Deierling et al. 2008; Gatlin and Goodman 2010). In the warning-decision environment, subjectively analyzed "lightning jumps" (i.e., forecaster subjectively determines a rapid increase in total lightning occurred in a short amount of time) can provide added confidence to forecasters on issuing convective warnings because there is a positive correlation between lightning jumps and severe weather (e.g., Schultz et al. 2009). Current lightning jump demonstrations are prototyping an automated lightning jump algorithm, developed by the University of Alabama in Huntsville and the National Severe Storms Laboratory, to provide the same information to forecasters objectively (Schultz et al. 2009, 2011). The pGLM observations also provide spatial lightning information and situational awareness for lightning safety as intracloud and cloud-to-cloud lightning often precede cloud-to-ground lightning (Stano 2012). Forecasters using the pGLM for incident support (e.g., outdoor events, airport and other transportation weather warnings, and storm surveys) can potentially provide threat information to customers, which can reduce the public's exposure to lightning. It is important to remember that the pGLM and total lightning observations are not intended as stand-alone resources, in that using this information with NEXRAD volume scans provides more insight about updraft characteristics and the resulting strength of a thunderstorm than does either dataset alone. The pGLM products have been evaluated at the AWT and HWT, while total lightning data have been evaluated at numerous WFOs and NWS Center Weather Service Units.

Overshooting top detection. Overshooting tops (OTs) that occur with strong convection and vigorous updrafts are composed of a small region of very cold IR BTs that are surrounded by a warmer cirrus anvil cloud. OTs occur because they continue to cool at a rate of 7–9 K km⁻¹ after they penetrate through the level of neutral buoyancy, making them much

colder than the adjacent anvil cloud, which resides somewhere between the level of neutral buoyancy and the tropopause (Adler and Mack 1986; Wang 2007). The overshooting cloud-top detection (OTD) algorithm first identifies a candidate OT that has IR BTs colder than the tropopause temperature predicted by a numerical weather prediction model (Bedka et al. 2010). Once this occurs, the cirrus anvil mean BT is computed using an approximate 8-km radius from the candidate OT. If the BT difference between the candidate OT and anvil mean BT exceeds 6.5 K, the candidate OT is flagged as an OT. These algorithm thresholds were based on a detailed analysis of OT and "enhanced V"-producing storms from 1-km Moderate Resolution Imaging Spectroradiometer (MODIS) and Advanced Very High Resolution Radiometer (AVHRR) observations. Feedback from the 2010 GOES-R Proving Ground suggested that the algorithm thresholds described by Bedka et al. (2010) were too conservative, causing some OT features to be missed. Therefore, to account for the current GOES series IR spatial resolution of 4 km, the required OTD thresholds for maximum OT IR temperature and OT-minus-anvil BT difference have been relaxed from 215.0 to 217.5 K and from 6.5 to 6.0 K, respectively.

The OTD product was developed initially to allow a forecaster to quickly identify vigorous convective updrafts that are associated with aviation weather hazards such as turbulence and lightning (Bedka et al. 2010). However, OTD evaluations within the GOES-R Proving Ground at the NOAA/Aviation Weather Center, HWT, the Storm Prediction Center, and the National Environmental Satellite, Data, and Information Service (NESDIS) Satellite Analysis Branch, as well as research by the algorithm developers, have revealed a number of other applications. For example, OT signatures were detected for approximately 55% of confirmed warm-season severe weather events across the United States between 2004 and 2009 and this indicates the product can increase situational awareness and forecaster confidence that a given storm is severe (Dworak et al. 2012). Forecasters in experimental test bed settings have found that a cessation of OTs in a mesoscale convective system or quasi-linear convective system can signal storm weakening prior to radar-based analysis, consistent with what was found in Dworak et al. (2012). Furthermore, many forecasters found the product to be especially useful at night when the lack of 1-km visible imagery can inhibit forecaster recognition of OTs. Other applications were associated with rapid tropical cyclone intensification and long-term

damaging-hail assessment. However, for the purposes of the forthcoming analysis, the OTDs will be used to diagnose the presence of intense convective updrafts.

On the day of a convective event the common meteorological guidance and observational datasets available to NWS meteorologists are shown in Fig. 1. Four to six hours before initial convective warnings, SPC convective outlooks, high-resolution model guidance, and upper-air soundings are, for example, used to assess the potential convective mode, location, and severity of convection later in the day. Three to five hours before warning operations commence, the synoptic-scale environment is often interrogated by completing manual analyses of aviation routine weather reports (METARs) and upper-air observations, as well as by using water vapor and IR imagery from GOES. A few hours before convection, the mesoscale environment can be analyzed using GOES 1-km visible imagery, METAR observations, gridded analyses such as those from the Real-Time Mesoscale Analysis (De Pondca et al. 2011) and Local Analysis and Prediction System (McGinley 1989), and hourly SPC mesoanalysis guidance (Bothwell et al. 2002). Also within this time frame, SPC mesoscale convective discussions are issued to describe an evolving severe weather threat, and convective watches are issued when the development of severe thunderstorms is imminent. With the exception of the

traditional tools described above, there is an overall lack of observational data that aids the mesoanalyst or warning forecaster in identifying short-term changes in the convective environment or storm structure and intensity, especially in the time period between the issuance of convective watches and warnings. The GOES-R convective toolkit product suite (shown using green timeline duration bars in Fig. 1) helps to address this information gap as each component has been shown to be useful to the warning forecaster in monitoring the preconvective environment and the overall severe weather potential. However, when the GOES-R products are used together to monitor the near-storm environment and storm intensity trends prior to and during a convective event, an additional level of situational awareness is provided. It should be noted that as the spatial and temporal resolution improvements associated with the GOES-R ABI are realized, the performance of the NearCast model, and the CI, CTC, and OTD products, may improve after GOES-R is operational. The remainder of this paper uses the 20 May 2013 severe weather outbreak as a case study to illustrate how integrating the aforementioned GOES-R convective products into a warning-decision-making framework can enhance near-storm environmental analysis, the warning-decision process for severe weather hazards, and overall forecaster situational awareness and confidence.

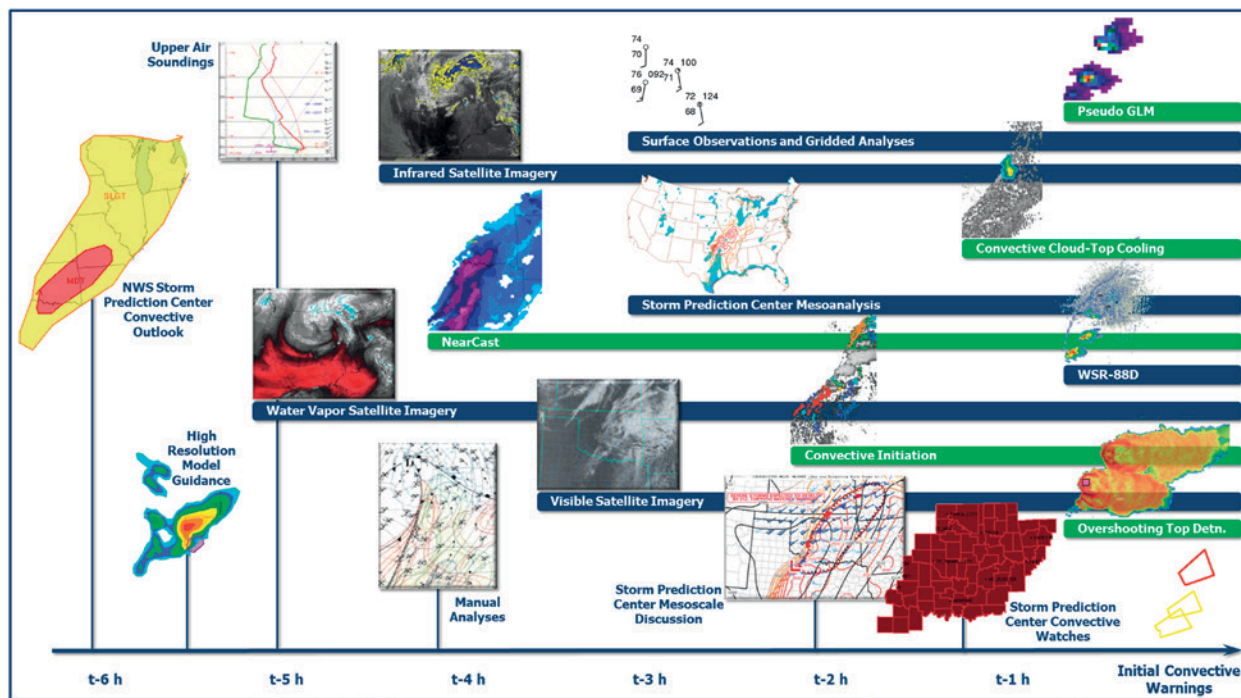


FIG. 1. Timeline depicting the common meteorological guidance and observational datasets available to NWS meteorologists (blue text and duration bars) and the GOES-R convective toolkit products (green duration bars) in the 6 h preceding a convective event.

20 MAY 2013 SEVERE WEATHER OUTBREAK.

The severe weather outbreak that occurred on 20 May 2013 produced wind damage, large hail, and tornadoes from Texas to Michigan. Several tornadoes occurred across central and southern Oklahoma with the strongest tornado occurring from Newcastle through Moore and the southern portion of Oklahoma City. This tornado was rated as a category 5 event on the enhanced Fujita scale (EF5; Burgess et al. 2014) and caused catastrophic damage along its 23-km-long path. The tornado was also responsible for 24 fatalities, 212 injuries, and more than \$2 billion in damage (NOAA/National Climatic Data Center 2013).

The synoptic-scale pattern responsible for the severe weather outbreak was well forecast by the SPC and the Norman, Oklahoma, NWS WFO (NOAA 2014). On 15 May, 6 days before the event, the SPC noted that 20 May had the highest tornado potential of the expected multiday severe weather outbreak and the Norman WFO hazardous weather outlook was highlighting the threat of severe weather and potentially strong tornadoes on 19–21 May. At 1200 UTC 20 May 2013, the synoptic-scale environment (not shown) across Oklahoma and the central United States was dominated by cyclonic flow aloft and a 65-knot (kt; 33.4 m s^{-1}) midlevel jet streak above an increasingly unstable air mass. To the east of a surface cold front that extended from western Minnesota south and southwestward through central Oklahoma and Texas, surface dewpoint temperatures were forecast to increase above 65°F (18°C) beneath an elevated mixed layer across Oklahoma by midday. The day-1 severe weather outlook issued by the SPC at 1217 UTC mentioned that supercellular convective storms with tornadoes and significant severe weather would be possible with the initial convection that was likely to develop by 2000 UTC.

In convective scenarios, uncertainty can exist in numerical model output with respect to the timing and location of the expected convection. The GOES-R NearCast, CI, and CTC products can be useful in addressing some of these model uncertainties. On the morning of 20 May 2013, the analysis of the GOES-R NearCast forecast cycle initialized at 1500 UTC revealed a reservoir of low-level moisture, as seen in the 900–700-hPa NearCast PW field (Fig. 2a), along a narrow axis immediately to the east of the cold front and moisture gradient across Oklahoma and Texas. Along the cold front, the greatest low-level moisture (>0.5 in. 900–700-hPa PW) in the NearCast analysis was located from near Lawton, Oklahoma, southwestward through the Red River valley, and into north-central Texas (Fig. 2a). Although the

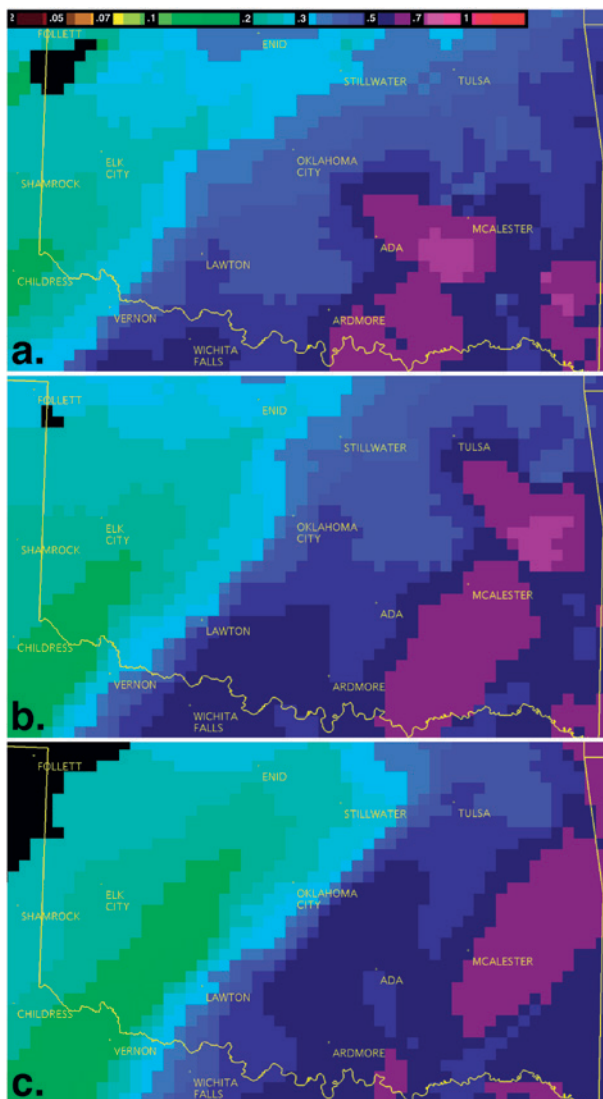


FIG. 2. (a) The 1500 UTC 20 May 2013 NearCast analysis of 900–700-hPa PW (in., shaded according to scale with greater moisture in warm colors). (b) As in (a), but for the 2-h forecast valid at 1700 UTC 20 May 2013. (c) As in (a), but for the 4-h forecast valid at 1900 UTC 20 May 2013.

northeastward extent of the greater low-level PW frontal axis was located near Lawton, the strongest midlevel convective instability (500–780-hPa θ_e difference) at this time was present to the south-southwest of Wichita Falls, Texas (Fig. 3a). The 2- and 4-h NearCast forecasts of low-level PW (Figs. 2b and 2c) show the leading edge of the moisture axis being transported to the northeast, located near Oklahoma City and Tulsa, Oklahoma, by 1700 and 1900 UTC, respectively. The extent of the increasing midlevel instability at 1700 UTC was forecast to be located near Lawton (Fig. 3b) and then Oklahoma City by 1900 UTC (Fig. 3c). Between 1500 and 1900 UTC,

just to the southeast of Lawton, the 500–780-hPa θ_e difference decreased from -4 to -13 K over the 4-h period (cf. Figs. 3a and 3c). Based on the 1500 UTC NearCast forecasts, support for the development and growth of convection would be maximized to the southwest of Oklahoma City, where the juxtaposition of the strengthening low-level moisture gradient (i.e., forcing) and increase in convective instability are forecast to occur by 1900 UTC.

The SPC issued a mesoscale discussion for southeastern Kansas, southwestern Missouri, and much of eastern Oklahoma to the east of the surface boundary

at 1726 UTC. Within the NWS WFO county warning area (CWA) for Norman, which covers the western two-thirds of Oklahoma excluding the panhandle (Fig. 4a), the mesoscale discussion stated that “an extremely volatile air mass exists with an increasing cumulus field from northwestern Texas into southwestern Oklahoma where strong heating persists.” At 1732 UTC, to the south of Oklahoma City near Lawton, the CI product indicated that convective initiation was likely in the next hour as probabilities were above 80% (Fig. 4a). Determining where convection is likely to develop when subjectively analyzing a cumulus field with existing observational datasets can be challenging for most forecasters. By using the guidance provided by the SPC and the probabilistic CI output, the mesoanalyst’s situational awareness can be initially focused to the southwest of Oklahoma City, within the Norman CWA.

Thirteen minutes later, at 1745 UTC, the CTC algorithm indicated a strong cooling rate, as defined by Sieglaff et al. (2014), of $-28^{\circ}\text{C} (15 \text{ min})^{-1}$ with the developing cumulus tower to the south of Lawton (Fig. 4b). This is significant because after analyzing 119 CTC detections, and their corresponding MESH values, Sieglaff et al. (2014) found that in an environment supportive of severe hail, developing convection having a CTC rate $< -20^{\circ}\text{C} (15 \text{ min})^{-1}$ is more likely to produce severe hail. Twenty-five minutes after the initial CTC signal was detected at 1811 UTC, the SPC issued the first tornado watch for central and eastern Oklahoma. At 1854 UTC, 70 min after the CTC detection, 4.5-cm (1.75 in.) hail was reported 6 mi (~ 10 km) north of Marlow, Oklahoma. It is important to note that the initial CI occurred along the midlevel moisture/instability discontinuity and the nose of the enhanced instability plume, which were forecast by the 1500 UTC NearCast model to be southwest of Oklahoma City between 1700 and 1900 UTC (Figs. 2 and 3). Farther to the south, CI probabilities continued to increase to $>90\%$ along the cold front between Wichita Falls and Vernon, Texas.

To the immediate west and southwest of Oklahoma City, CI probabilities increased to 45% at 1815 UTC (not shown) and then to 61% and 63% at 1825 (not shown) and 1832 UTC (Fig. 5a), respectively. This was the first GOES-R CI product signal, since convection was not yet detected on the Weather Surveillance Radar-1988 Doppler (WSR-88D) near Oklahoma City (KTLX), that CI could occur in the next hour west of Oklahoma City. Approximately 40 min later, at 1910 UTC, an extreme $-61^{\circ}\text{C} (15 \text{ min})^{-1}$ CTC rate was detected (Fig. 5b) in the same area where elevated CI probabilities occurred (Fig. 5a). In addition,

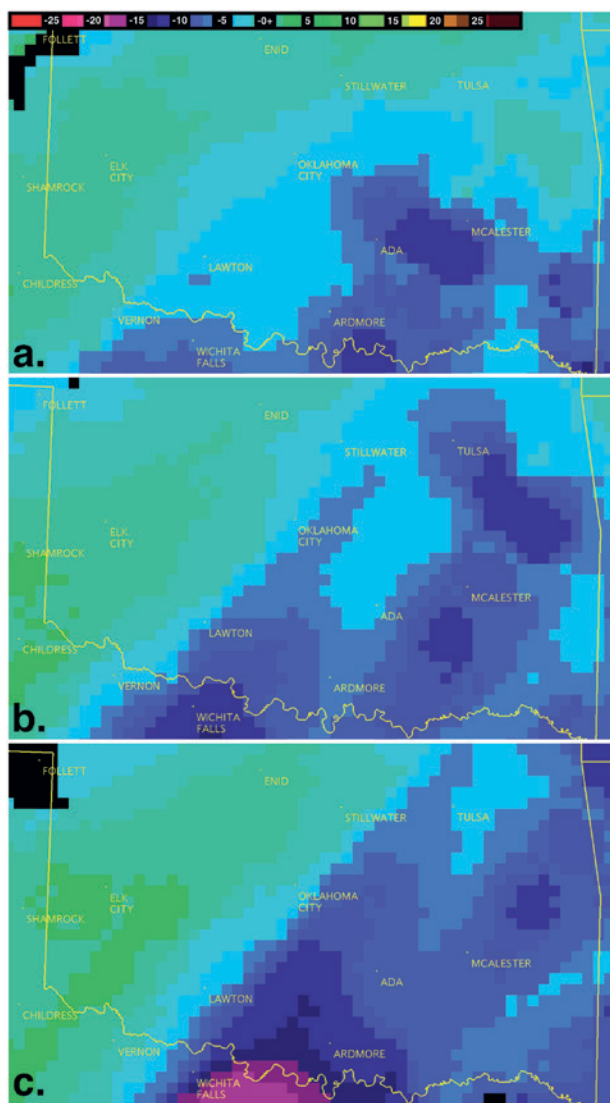


FIG. 3. (a) The 1500 UTC 20 May 2013 NearCast analysis of equivalent potential temperature difference (500–780 hPa, shaded according to scale with convective instability in cool colors and convective stability in warm colors). (b) As in (a), but for the 2-h forecast valid at 1700 UTC 20 May 2013. (c) As in (a), but for the 4-h forecast valid at 1900 UTC 20 May 2013.

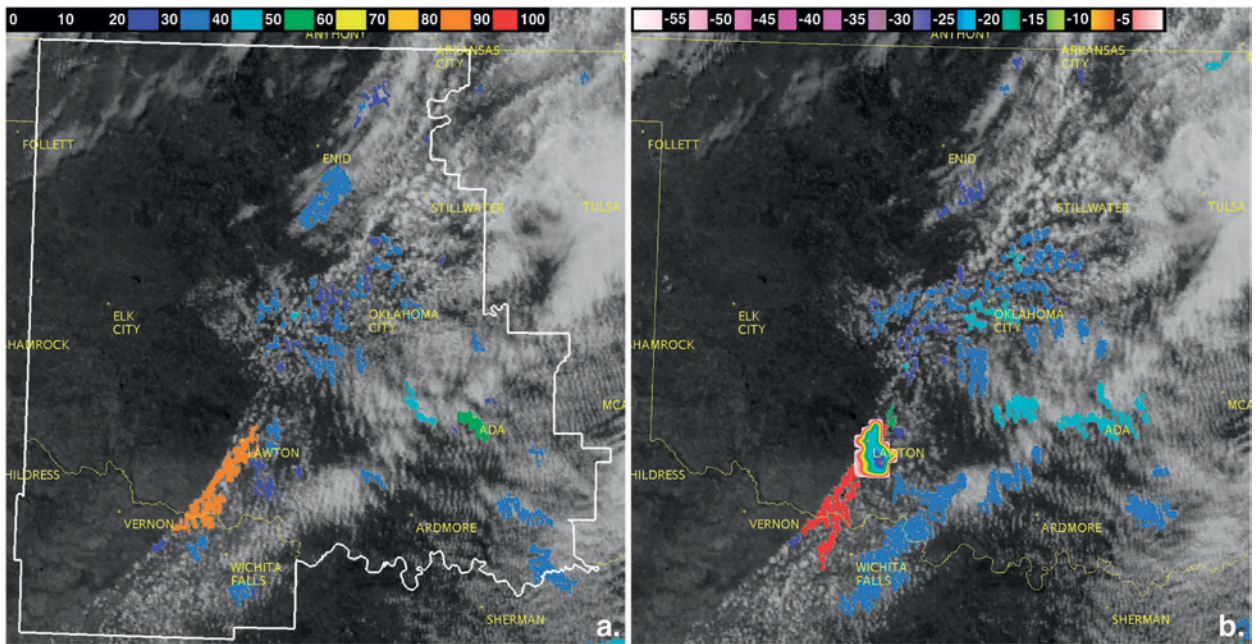


FIG. 4. (a) The 1732 UTC 20 May 2013 visible satellite image from GOES-13 and CI (%) ,shaded according to scale). **(b)** As in (a), but with convective CTC [$^{\circ}\text{C}$ (15 min) $^{-1}$], shaded according to scale] valid at 1745 UTC 20 May 2013. The Norman NWS CWA boundary is shown in (a).

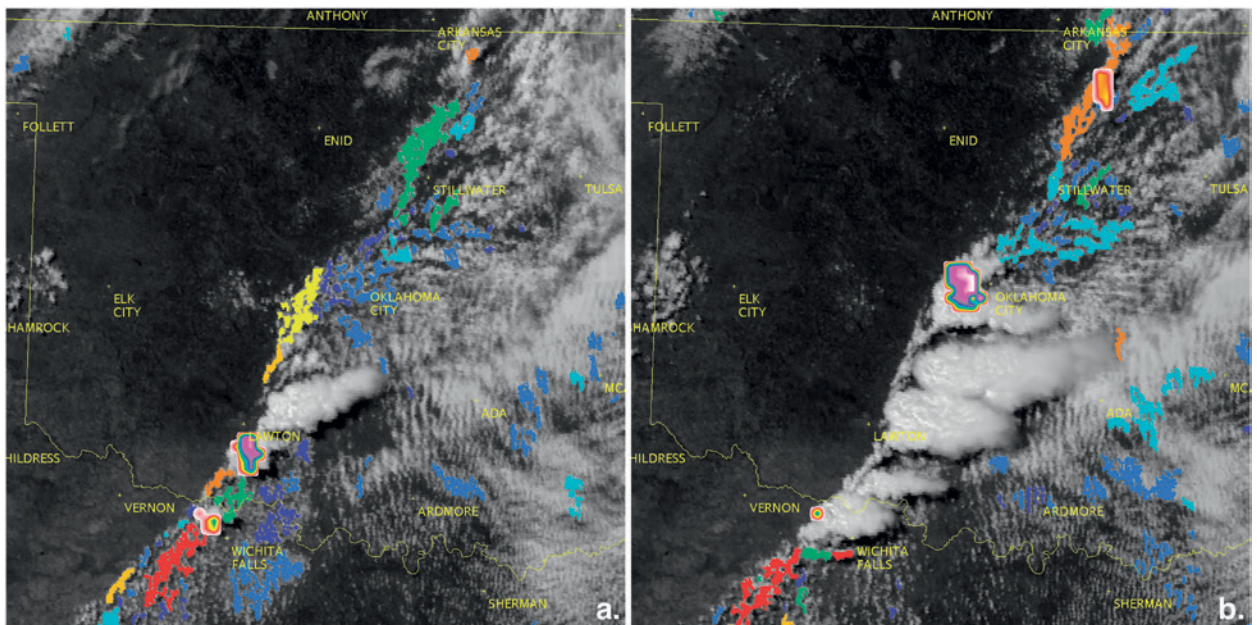


FIG. 5. (a) As in Fig. 4b, but valid at 1832 UTC 20 May 2013. **(b)** As in (a), but valid at 1910 UTC 20 May 2013.

between 1906 (Fig. 6a) and 1910 UTC (Fig. 7a), pGLM flash extent density observations indicated that a 32 flash per minute lightning jump had occurred [for a quantitative time series of this lightning jump, see Stano et al. (2014)]. As this was taking place, the maximum 0.5° radar reflectivity from the KTLX WSR-88D increased from 33 to 56 dBZ between 1904

and 1912 UTC (Figs. 6b and 7b) and, for reference, the first severe thunderstorm warning was issued for this storm at 1912 UTC by the Norman WFO. Along the cold front, to the north between Arkansas City, Kansas, and Tulsa and to the southwest of Wichita Falls, CI probabilities increased to >80%, which indicated additional thunderstorm development was

likely in these areas (Fig. 5b). By integrating these datasets into the real-time observational analysis of a mesoanalyst or warning forecaster, they can develop more confidence in where CI is anticipated and that thunderstorm updrafts are rapidly strengthening.

During severe weather warning operations at NWS WFOs, the mesoanalyst and/or warning forecaster often uses one of their monitors to display observational datasets (e.g., satellite and METARs; SPC mesoanalysis fields) for near-storm environmental analysis. This allows them to monitor trends in satellite imagery and other observations for changes in atmospheric conditions that may affect the development of convection, its intensity, and evolution. By synergistically using the GOES-R convective products, a more complete environmental and convective storm analysis display can be developed for NWS operations. Displays of various parameters using the Advanced Weather Interactive Processing System-2 (AWIPS-2), which is currently replacing AWIPS-1 as the baseline visualization and analysis platform at WFOs across the country, are configurable to allow the user the opportunity to develop unique

combinations of meteorological data. For example, in Fig. 8a the θ_e difference forecasts from the NearCast model are combined with the GOES-13 visible imagery to diagnose the pattern and magnitude of convective instability, including locations of gradients, maxima, and minima. In Fig. 8b, the CI, CTC, and OTD products are combined with visible imagery to identify where convective cores are developing, how quickly they are strengthening, and how intense they are becoming. The pGLM flash extent density observations are combined with satellite imagery in Fig. 8c to quantify total storm electrification, and in Figs. 8d and 8e, the 0.5° radar reflectivity and storm-relative velocity allow the user to compare the GOES-R products and satellite imagery with radar features. Integrating satellite imagery and products with radar data to develop multiparameter displays, similar to those presented here, help meteorologists achieve heightened situational awareness, convective warning confidence, and a more comprehensive representation of the physical processes relevant to convection that are occurring in the atmosphere.

At 1930 UTC, the 30-min forecast of NearCast θ_e difference from the 1900 UTC initialization shows the northeastward extent of the near-frontal axis of

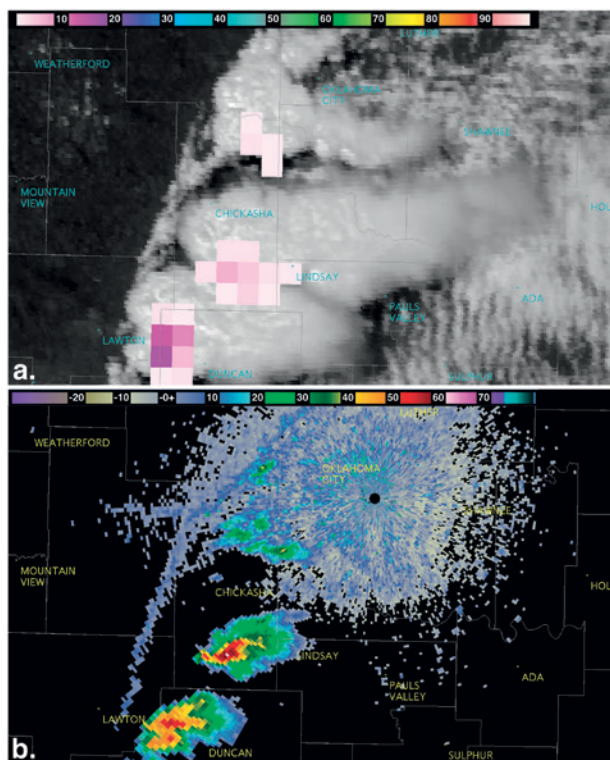


FIG. 6. (a) The 1900 UTC 20 May 2013 visible satellite image from GOES-13 and the 1906 UTC 20 May 2013 pGLM flash extent density [flashes $(64 \text{ km})^{-2} \text{ min}^{-1}$, shaded according to scale] and (b) 1904 UTC 20 May 2013 KTLX WSR-88D 0.5° reflectivity (dBZ, shaded according to the scale).

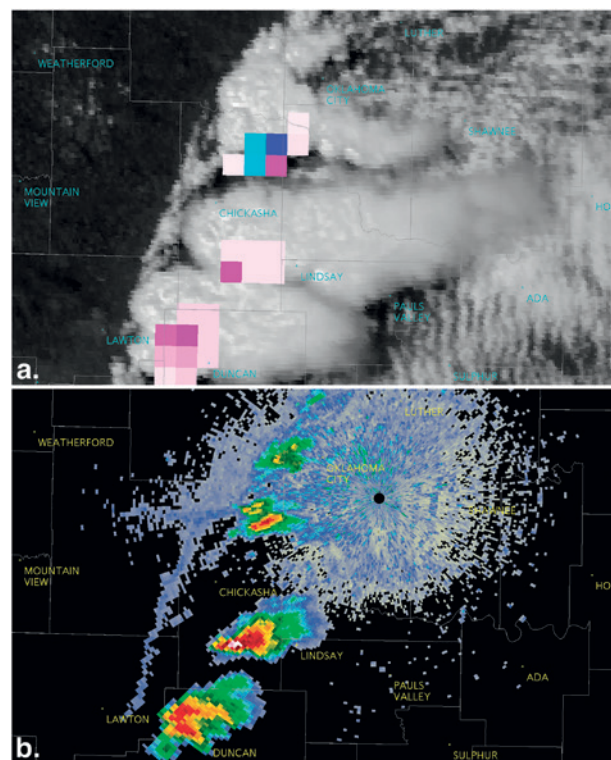


FIG. 7. (a) As in Fig. 6a, but visible satellite image valid at 1907 UTC 20 May 2013 and pGLM flash extent density valid at 1910 UTC 20 May 2013. (b) As in Fig. 6b, but valid at 1912 UTC 20 May 2013.

stronger convective instability had reached an area just to the southeast of Oklahoma City (Fig. 8a). The *GOES-13* visible satellite image indicated thunderstorms developing near the midlevel moisture/instability discontinuity, previously discussed with respect to the NearCast forecasts in Figs. 2 and 3. The most intense updrafts at this time, identified by the OTD algorithm (pink pixels in Fig. 8b), were located to the west-southwest of Oklahoma City and east of Lawton. Severe thunderstorm warnings were in effect for both of these thunderstorms at 1932 UTC.

Between 1938 (Fig. 8c) and 1951 UTC (Fig. 9c), a second subjective lightning jump occurred as the pGLM flash extent density observations increased from 19 to 55 flashes per minute. This provided indication that the thunderstorm's updraft within the mixed-phase region of the cloud was undergoing additional strengthening, and the warning forecaster can use the increase in total lightning to infer rapidly increasing updraft strength (Stano et al. 2014). When comparing the pGLM observations (Fig. 9c) to the 0.5° radar reflectivity and storm-relative velocity from the KTLX WSR-88D at 1951 UTC (Figs. 9d and

9e), the pixel with the most flashes (olive filled and outlined in black) is collocated with the updraft on radar and with the detected OT in Fig. 9b. In addition, the maximum gate-to-gate shear increased from 36.9 to 61.2 kt (19.0–31.5 m s⁻¹) during the lightning jump as the updraft strengthened and stretched. This confirms the presence of an intense rotating updraft (denoted by the WSR-88D rotational velocity couplet in Fig. 9e) with different observation sources before the tornado was first observed at 1956 UTC. Although the Norman WFO issued a tornado warning at 1940 UTC, the increase in total lightning observations and the presence of an OT would have most likely complemented the warning forecaster's elevated awareness of this unfolding high-impact situation while enhancing convective warning confidence.

CONCLUSIONS. An initial NWS forecaster evaluation of the fused GOES-R integrated convective product display was completed by participants at the 2014 Spring Experiment of the NOAA HWT (Line 2014). The primary goal of the evaluation was to demonstrate the value of quickly viewing multiple

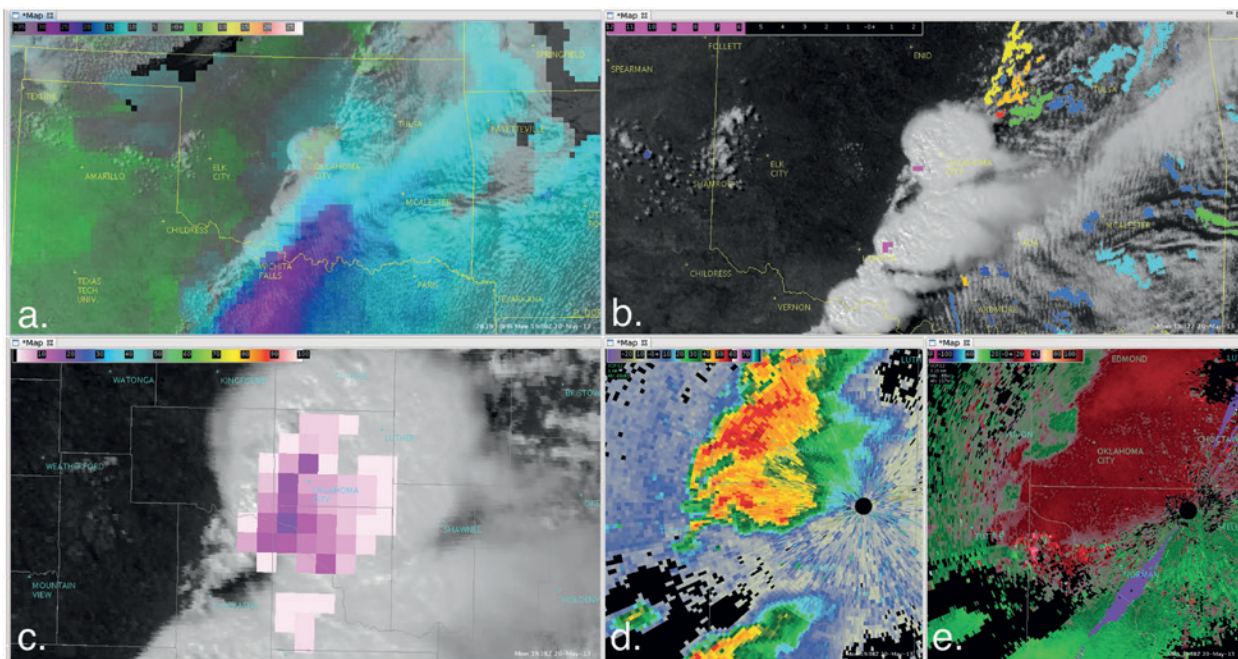


FIG. 8. (a) The 1932 UTC 20 May 2013 visible satellite image from *GOES-13* and 1900 UTC 20 May 2013 NearCast 30-min forecast of equivalent potential temperature difference (500 – 780 hPa, shaded according to scale with convective instability in cool colors) valid at 1930 UTC 20 May 2013. (b) The 1932 UTC 20 May 2013 visible satellite image from *GOES-13*, CI (%), shaded according to scale), convective CTC [°C (15 min)⁻¹, shaded according to scale], and overshooting top detection (pink pixels). (c) The 1937 UTC 20 May 2013 visible satellite image from *GOES-13* and the 1938 UTC 20 May 2013 pGLM flash extent density [flashes (64 km)² min⁻¹, shaded according to scale]. (d) The 1938 UTC 20 May 2013 KTLX WSR-88D 0.5° reflectivity (dBZ, shaded according to the scale). (e) The 1938 UTC 20 May 2013 KTLX WSR-88D 0.5° storm-relative velocity (kt, 1 kt = 0.51 m s⁻¹ shaded according to the scale).

satellite products and other observational data simultaneously. The majority of HWT participants quickly understood the enhanced value of viewing and analyzing the products in unison, consistently using the integrated display during experimental warning operations throughout each week. After using the display, one forecaster commented: “Overall, I think this procedure will be of operational use, especially once GOES-R is actually launched and these products increase in overall utility.” Once forecasters were comfortable using the display, they were encouraged to make modifications to the approach based on their own decision-making processes. Therefore, a secondary goal of the evaluation was to observe these modifications and seek feedback on methods to more efficiently and effectively integrate observational data into the warning process. Not surprisingly, forecasters added datasets such as METARs and products from the National Severe Storms Laboratory’s Multi-Radar/Multi-Sensor System (Lakshmanan et al. 2006). The authors understand that the fused GOES-R displays shown in Figs. 5 and 6 would most likely be modified by users for personal preference and different convective situations. In the end, it is the effective practice of incorporating numerous observational datasets into mesoanalysis and warning operations that is of utmost importance.

Not discussed in this paper is the impact that increased spectral, temporal, and spatial resolution

may have on these future capability products once GOES-R is launched. In particular, if the algorithms produce satellite-derived information as frequently as every minute (depending on the GOES-R scanning strategy), it is possible the performance of the algorithms described herein may evolve and supplemental capabilities may be realized. For example, for a 2-week period (8–25 May 2014) the *GOES-14* imager was placed in an experimental rapid-scan 1-min mode to simulate the temporal capability of GOES-R (Schmit et al. 2013, 2015). Using the 1-min data on 10 May 2014, the CTC algorithm was processed every minute and the output (not shown) revealed that, over a period of almost 45 min, numerous weak CTC detections [$>-15^{\circ}\text{C}(\text{min})^{-5}$] preceded stronger detections [$<-20^{\circ}\text{C}(\text{min})^{-5}$] prior to the development of severe thunderstorms. It is speculated that the numerous weaker detections were an indication that the convective inhibition was eroding in a discontinuous manner before stronger cumulus development commenced (i.e., stronger CTC detections). Although this example shows that incorporating GOES-R data into the algorithms may have some effect on their performance, the algorithms are designed to be flexible enough that the current versions can prepare the forecaster for the GOES-R era.

The focus of the GOES-R Proving Ground is twofold: to provide feedback on demonstration product performance to developers in an effort to

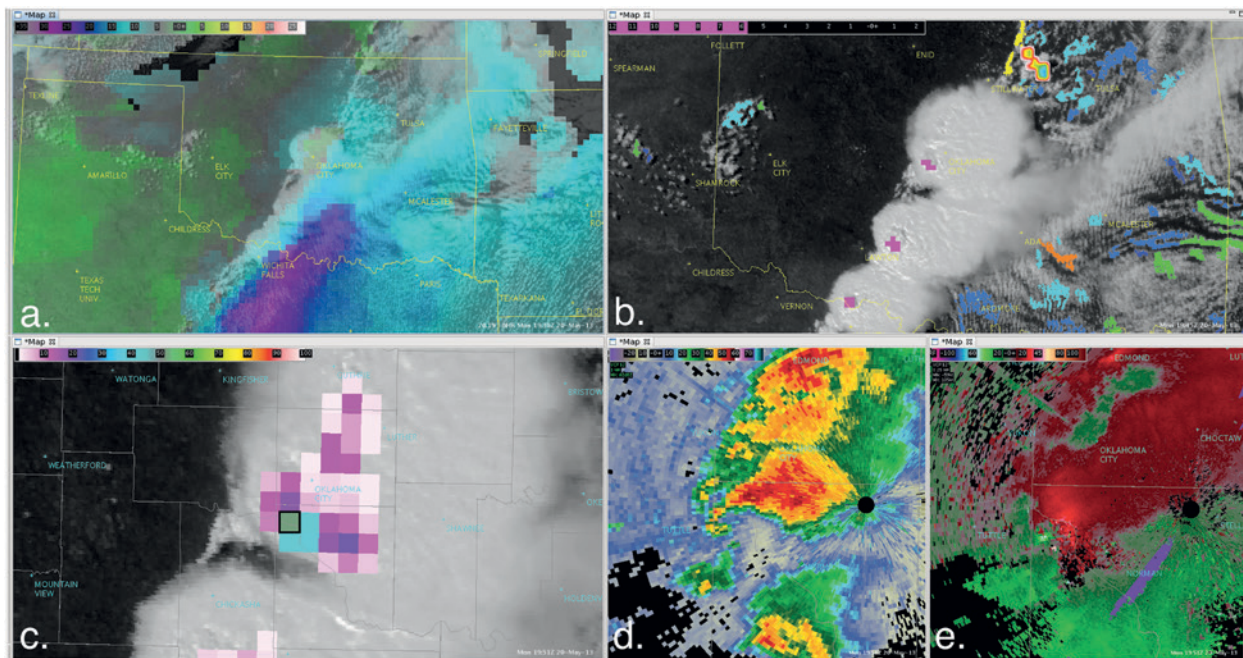


FIG. 9. (a),(b) As in Figs. 5a and 5b, respectively, but valid at 1945 UTC 20 May 2013. (c) As in Fig. 5c, but with pGLM flash extent density valid at 1951 UTC 20 May 2013. (d) As in Fig. 5d, but valid at 1951 UTC 20 May 2013. (e) As in Fig. 5e, but valid at 1951 UTC 20 May 2013.

complete the research-to-operations loop and to prepare the user communities for the future capabilities of GOES-R. To date, the majority of the evaluations have been product centric (i.e., forecasters at a WFO, NOAA test bed, or a national center evaluate and provide feedback on individual products). As the launch of GOES-R approaches, the development of methods and effective practices that combine GOES-R products with other sources of short-term information that are directly integrated into the forecaster environment is important. By developing a fused environmental and storm attribute decision-aid display that is easy to use and interpret, forecasters can gain an improved understanding of the convective environment and how specific convective storms are developing in an efficient and effective way. In turn, forecasters can more easily extract the most important information as a convective event evolves, which is critical to NWS's core partners, decision makers, and the general public.

Even though the example presented in this paper is a high-impact severe weather event, the synergistic approach of using GOES-R convective product capabilities together is applicable in all situations where convection may develop or already exists. These products supplement existing observational datasets and provide forecasters with critical information in the time period from when cumulus clouds first develop, to when a convective watch is issued, to when warning operations begin. Furthermore, the concept of incorporating GOES-R capabilities into a situational awareness display allows users to quickly diagnose a more complete physical depiction of short-term changes in the atmosphere that in turn allows forecasters to make better decisions on where and when to issue warnings that help save lives and property across the United States.

ACKNOWLEDGMENTS. The authors thank Steven Weiss (NOAA/NWS/Storm Prediction Center), Dave Radell (NOAA/NWS, Eastern Region Headquarters), Jeffrey Craven (NOAA/NWS, Milwaukee/Sullivan, Wisconsin), and Frank Alsheimer (NOAA/NWS, Charleston, South Carolina) for their reviews of earlier versions of this manuscript and the three anonymous reviewers and the journal editor, who provided thorough comments that improved the final version of this paper. Funding is supported by a NOAA/STAR GOES-R Proving Ground grant; a GOES Improved Measurements and Products Activities Plan grant under NOAA–University of Wisconsin Cooperative Agreement NA10NES440001, the U.S. Department of Commerce; NOAA Grant NA11NES4400014, U.S. Department of Commerce; and NOAA GOES-R Algorithm Working Group Grant NA06NES4400002, U.S. Department of Commerce.

REFERENCES

- Adler, R. F., and R. A. Mack, 1986: Thunderstorm cloud top dynamics as inferred from satellite observations and a cloud top parcel model. *J. Atmos. Sci.*, **43**, 1945–1960, doi:10.1175/1520-0469(1986)043<1945:TCTDAI>2.0.CO;2.
- Bedka, K., J. Brunner, R. Dworak, W. Feltz, J. Otkin, and T. Greenwald, 2010: Objective satellite-based detection of overshooting tops using infrared window channel brightness temperature gradients. *J. Appl. Meteor. Climatol.*, **49**, 181–202.
- Berendes, T. A., J. R. Mecikalski, W. M. Mackenzie, K. M. Bedka, and U. S. Nair, 2008: Convective cloud detection in satellite imagery using standard deviation limited adaptive clustering. *J. Geophys. Res.*, **113**, D20207, doi:10.1029/2008JD010287.
- Bothwell, P. D., J. A. Hart, and R. L. Thompson, 2002: An integrated three-dimensional objective analysis scheme in use at the Storm Prediction Center. Preprints, *21st Conf. on Severe Local Storms/19th Conf. on Weather Analysis and Forecasting/15th Conf. on Numerical Weather Prediction*, San Antonio, TX, Amer. Meteor. Soc., J117–J120. [Available online at <https://ams.confex.com/ams/pdfpapers/47482.pdf>]
- Browning, K. A., and D. Atlas, 1965: Initiation of precipitation in vigorous convective clouds. *J. Atmos. Sci.*, **22**, 678–683, doi:10.1175/1520-0469(1965)022<0678:IOPIVC>2.0.CO;2.
- Burgess, D., and Coauthors, 2014: 20 May 2013 Moore, Oklahoma, tornado: Damage survey and analysis. *Wea. Forecasting*, **29**, 1229–1237, doi:10.1175/WAF-D-14-00039.1.
- Caplan, P., J. Derber, W. Gemmill, S.-Y. Hong, H.-L. Pan, and D. Parrish, 1997: Changes to the 1995 NCEP operational Medium-Range Forecast model analysis–forecast system. *Wea. Forecasting*, **12**, 581–594, doi:10.1175/1520-0434(1997)012<0581:CTTNOM>2.0.CO;2.
- Clark, A. J., and Coauthors, 2012: An overview of the 2010 Hazardous Weather Testbed Experimental Forecast Program Spring Experiment. *Bull. Amer. Meteor. Soc.*, **93**, 55–74, doi:10.1175/BAMS-D-11-00040.1.
- Deierling, W., W. A. Petersen, J. Latham, S. Ellis, and H. J. Christian, 2008: The relationship between lightning activity and ice fluxes in thunderstorms. *J. Geophys. Res.*, **113**, D15210, doi:10.1029/2007JD009700.
- De Ponca, M. S. F. V., and Coauthors, 2011: The real-time mesoscale analysis at NOAA's National Centers for Environmental Prediction: Current status and development. *Wea. Forecasting*, **26**, 593–612, doi:10.1175/WAF-D-10-05037.1.

- Dworak, R., K. M. Bedka, J. Brunner, and W. Feltz, 2012: Comparison between GOES-12 overshooting top detections, WSR-88D radar reflectivity, and severe storm reports. *Wea. Forecasting*, **27**, 684–699, doi:10.1175/WAF-D-11-00070.1.
- Gatlin, P., and S. J. Goodman, 2010: A total lightning trending algorithm to identify severe thunderstorms. *J. Atmos. Oceanic Technol.*, **27**, 3–22, doi:10.1175/2009JTECHA1286.1.
- Goodman, S. J., and Coauthors, 2012: The GOES-R proving ground: Accelerating user readiness for the next-generation geostationary environmental satellite system. *Bull. Amer. Meteor. Soc.*, **93**, 1029–1040, doi:10.1175/BAMS-D-11-00175.1.
- , and Coauthors, 2013: The GOES-R Geostationary Lightning Mapper (GLM). *Atmos. Res.*, **125–126**, 34–49, doi:10.1016/j.atmosres.2013.01.006.
- Hannon, S., L. L. Strow, and W. W. McMillan, 1996: Atmospheric infrared fast transmittance models: A comparison of two approaches. *Optical Spectroscopic Techniques and Instrumentation for Atmospheric and Space Research II*, P. B. Hays and J. Wang, Eds., International Society for Optical Engineering, (SPIE Proceedings, Vol. 2830), 94–105, doi:10.1117/12.256106.
- Heidinger, A. K., and M. J. Pavolonis, 2009: Gazing at cirrus clouds for 25 years through a split window. Part I: Methodology. *J. Appl. Meteor. Climatol.*, **48**, 1100–1116, doi:10.1175/2008JAMC1882.1.
- Hosmer, D. W., and S. Lemeshow, 1989: *Applied Logistic Regression*. John Wiley and Sons, 307 pp.
- Kuhlman, K. M., C. L. Ziegler, E. R. Mansell, D. R. MacGorman, and J. M. Straka, 2006: Numerically simulated electrification and lightning of the 29 June STEPS supercell storm. *Mon. Wea. Rev.*, **134**, 2734–2757, doi:10.1175/MWR3217.1.
- Lakshmanan, V., T. Smith, K. Hondl, G. J. Stumpf, and A. Witt, 2006: A real-time, three-dimensional, rapidly updating, heterogeneous radar merger technique for reflectivity, velocity, and derived products. *Wea. Forecasting*, **21**, 802–823, doi:10.1175/WAF942.1.
- Lennon, C. L., 1975: LDAR—A new lightning detection and ranging system. *Eos, Trans. Amer. Geophys. Union*, **56**, 991.
- Levit, J. J., B. Entwistle, and C. Wallace, 2011: The Aviation Weather Testbed: Infusion of new science and technology for aviation operations. *Second Aviation, Range, and Aerospace Meteorology Special Symp. on Weather–Air Traffic Management Integration*, Seattle, WA, Amer. Meteor. Soc., 3.3. [Available online at <https://ams.confex.com/ams/pdffpapers/185616.pdf>.]
- Lhermitte, R., and P. R. Krehbiel, 1979: Doppler radar and radio observations of thunderstorms. *IEEE Trans. Geosci. Electron.*, **17**, 162–171, doi:10.1109/TGE.1979.294644.
- Line, W. E., 2013: Using isentropic techniques to improve the utility of GOES moisture observations. M.S. thesis, Dept. of Atmospheric and Oceanic Sciences, University of Wisconsin–Madison, 77 pp.
- , 2014: GOES-R Proving Ground demonstration at the Hazardous Weather Testbed 2014 Spring Experiment final evaluation. NOAA GOES-R Proving Ground, 36 pp. [Available online at www.goes-r.gov/users/docs/pg-activities/PGFR-HWT-2014-Final.pdf.]
- Maggio, C., and Coauthors, 2005: Lightning-initiation locations as a remote sensing tool of large thunderstorm electric field vectors. *J. Atmos. Oceanic Technol.*, **22**, 1059–1068, doi:10.1175/JTECH1750.1.
- Maier, L. M., C. Lennon, T. Britt, and S. Schaefer, 1995: Lightning Detection and Ranging (LDAR) system performance analysis. Preprints, *Sixth Conf. on Aviation Weather Systems*, Dallas, TX, Amer. Meteor. Soc., 305–309.
- McCaul, E. W., Jr., J. Bailey, J. Hall, S. J. Goodman, R. J. Blakeslee, and D. E. Buechler, 2005: A flash clustering algorithm for North Alabama Lightning Mapping Array data. *Conf. on Meteorological Applications of Lightning Data*, San Diego, CA, Amer. Meteor. Soc., 5.3. [Available online at https://ams.confex.com/ams/Annual2005/techprogram/paper_84373.htm.]
- , S. J. Goodman, K. M. LaCasse, and D. J. Cecil, 2009: Forecasting lightning threat using cloud-resolving model simulations. *Wea. Forecasting*, **24**, 709–729, doi:10.1175/2008WAF2222152.1.
- McGinley, J. A., 1989: The Local Analysis and Prediction System. Preprints, *12th Conf. on Weather Analysis and Forecasting*, Monterey, CA, Amer. Meteor. Soc., 15–20.
- Mecikalski, J. R., and K. M. Bedka, 2006: Forecasting convective initiation by monitoring the evolution of moving cumulus daytime GOES imagery. *Mon. Wea. Rev.*, **134**, 49–78, doi:10.1175/MWR3062.1.
- , S. J. Paech, K. M. Bedka, and L. A. Litten, 2008: A statistical evaluation of GOES cloud-top properties for nowcasting convective initiation. *Mon. Wea. Rev.*, **136**, 4899–4914, doi:10.1175/2008MWR2352.1.
- , P. D. Watts, and M. Koenig, 2011: Use of Meteosat Second Generation optimal cloud analysis fields for understanding physical attributes of growing cumulus clouds. *Atmos. Res.*, **102**, 175–190, doi:10.1016/j.atmosres.2011.06.023.
- , P. Minnis, and R. Palikonda, 2013: Use of satellite derived cloud properties to quantify growing cumulus beneath cirrus clouds. *Atmos. Res.*, **120–121**, 192–201, doi:10.1016/j.atmosres.2012.08.017.

- , J. K. Williams, C. P. Jewett, D. Ahijevych, A. LeRoy, and J. R. Walker, 2015: Probabilistic 0–1-h convective initiation nowcasts that combine geostationary satellite observations and numerical weather prediction model data. *J. Appl. Meteor. Climatol.*, **54**, 1039–1059, doi:10.1175/JAMC-D-14-0129.1.
- Mueller, C., T. Saxen, R. Roberts, J. Wilson, T. Betancourt, S. Dettling, N. Oien, and J. Yee, 2003: NCAR Auto-Nowcast System. *Wea. Forecasting*, **18**, 545–561, doi:10.1175/1520-0434(2003)018<0545:NAS>2.0.CO;2.
- NOAA/National Climatic Data Center, 2013: Storm Events Database. Subset used: May 2013, accessed 8 August 2013.
- NOAA, 2014: May 2013 Oklahoma tornadoes and flash flooding. NWS Service Assessment, 62 pp. [Available online at www.nws.noaa.gov/om/assessments/pdfs/13oklahoma_tornadoes.pdf.]
- Petersen, R. A., R. Aune, and T. Rink, 2010: Objective short-range forecasts of the pre-convective environment using SEVIRI data. *2010 EUMETSAT Meteorological Satellite Conf.*, Cordoba, Spain, EUMETSAT. [Available online at www.eumetsat.int/website/home/News/ConferencesandEvents/DAT_2042511.html.]
- , —, and —, 2011: Enhancing objective short-range forecasts of the pre-convective environment using SEVIRI data. *2011 EUMETSAT Meteorological Satellite Conf.*, Oslo, Norway, EUMETSAT. [Available online at www.eumetsat.int/website/home/News/ConferencesandEvents/DAT_2039705.html.]
- , W. Line, R. Aune, W. Straka, and R. Dworak, 2013: Improving very-short-range forecasts of the pre-convective environment using clear-air SEVIRI products. *2013 EUMETSAT Meteorological Satellite Conf./19th Conf. on Satellite Meteorology, Oceanography, and Climatology, Vienna, Austria, EUMETSAT/Amer. Meteor. Soc.* [Available online at www.eumetsat.int/website/home/News/ConferencesandEvents/DAT_2027670.html.]
- Proctor, D. E., 1971: A hyperbolic system for obtaining VHF radio pictures of lightning. *J. Geophys. Res.*, **76**, 1478–1489, doi:10.1029/JC076i006p01478.
- , 1981: VHF radio pictures of cloud flashes. *J. Geophys. Res.*, **86**, 4041–4071, doi:10.1029/JC086iC05p04041.
- Purdum, J. F. W., 1976: Some uses of high-resolution GOES imagery in the mesoscale forecasting of convection and its behavior. *Mon. Wea. Rev.*, **104**, 1474–1483, doi:10.1175/1520-0493(1976)104<1474:SUOHGR>2.0.CO;2.
- , 1982: Subjective interpretations of geostationary satellite data for nowcasting. *Nowcasting*, K. Browning, Ed., Academic Press, 149–166.
- Ralph, F. M., and Coauthors, 2013: The emergence of weather-focused test beds linking research and forecasting operations. *Bull. Amer. Meteor. Soc.*, **94**, 1187–1210, doi:10.1175/BAMS-D-12-00080.1.
- Rison, W., R. J. Thomas, P. R. Krehbiel, T. Hamlin, and J. Harlin, 1999: A GPS-based three-dimensional lightning mapping system: Initial observations in central New Mexico. *Geophys. Res. Lett.*, **26**, 3573–3576, doi:10.1029/1999GL010856.
- Roberts, R. D., and S. Rutledge, 2003: Nowcasting storm initiation and growth using GOES-8 and WSR-88D data. *Wea. Forecasting*, **18**, 562–584.
- Schmit, T. J., M. M. Gunshor, W. P. Menzel, J. Li, S. Bachmeier, and J. J. Gurka, 2005: Introducing the next-generation Advanced Baseline Imager (ABI) on GOES-R. *Bull. Amer. Meteor. Soc.*, **86**, 1079–1096, doi:10.1175/BAMS-86-8-1079.
- , J. Li, J. Li, W. F. Feltz, J. J. Gurka, M. D. Goldberg, and K. J. Schrab, 2008: The GOES-R Advanced Baseline Imager and the continuation of current sounder products. *J. Appl. Meteor. Climatol.*, **47**, 2696–2711, doi:10.1175/2008JAMC1858.1.
- , and Coauthors, 2013: Geostationary operational environmental satellite (GOES)-14 super rapid scan operations to prepare for GOES-R. *J. Appl. Remote Sens.*, **7**, 073462, doi:10.1117/1.JRS.7.073462.
- , and Coauthors, 2015: Rapid Refresh imagery of significant events: Preparing users for the next generation of geostationary operational satellites. *Bull. Amer. Meteor. Soc.*, doi:10.1175/BAMS-D-13-00210.1, in press.
- Schultz, C. J., W. A. Petersen, and L. D. Carey, 2009: Preliminary development and evaluation of lightning jump algorithms for the real-time detection of severe weather. *J. Appl. Meteor. Climatol.*, **48**, 2543–2563, doi:10.1175/2009JAMC2237.1.
- , —, and —, 2011: Lightning and severe weather: A comparison between total and cloud-to-ground lightning trends. *Wea. Forecasting*, **26**, 744–755, doi:10.1175/WAF-D-10-05026.1.
- Sieglauff, J. M., L. M. Counce, W. F. Feltz, K. M. Bedka, M. J. Pavolonis, and A. K. Heidinger, 2011: Nowcasting convective storm initiation using satellite-based box-averaged cloud-top cooling and cloud-type trends. *J. Appl. Meteor. Climatol.*, **50**, 110–126, doi:10.1175/2010JAMC2496.1.
- , —, and —, 2014: Improving satellite-based convective cloud growth monitoring with visible optical depth retrievals. *J. Appl. Meteor. Climatol.*, **53**, 506–520, doi:10.1175/JAMC-D-13-0139.1.
- Stano, G. T., 2012: Using total lightning observations to enhance lightning safety. *Seventh Symp. on Policy and Socio-Economic Research*, New Orleans, LA,

- Amer. Meteor. Soc., 327. [Available online at <https://ams.confex.com/ams/92Annual/webprogram/Paper202740.html>.]
- , C. J. Schultz, L. D. Carey, D. R. MacGorman, and K. M. Calhoun, 2014: Total lightning observations and tools for the 20 May 2013 Moore, Oklahoma, tornadic supercell. *J. Oper. Meteor.*, **2**, 71–88, doi:10.15191/nwajom.2014.0207.
- Terborg, A., and C. M. Gravelle, 2012: Aviation Weather Testbed 2012 Summer Experiment GOES-R desk final evaluation. GOES-R Proving Ground, 20 pp. [Available online at www.goes-r.gov/users/docs/pg-activities/PGFR-AWC-2012-Final.pdf.]
- Tessendorf, S. A., L. J. Miller, K. C. Wiens, and S. A. Rutledge, 2005: The 29 June 2000 supercell observed during STEPS. Part I: Kinematics and microphysics. *J. Atmos. Sci.*, **62**, 4127–4150, doi:10.1175/JAS3585.1.
- Thomas, R. J., P. R. Krehbiel, W. Rison, S. Hunyady, W. Winn, T. Hamlin, and J. Harlin, 2004: Accuracy of the Lightning Mapping Array. *J. Geophys. Res.*, **109**, D14207, doi:10.1029/2004JD004549.
- Walker, J. R., W. M. MacKenzie Jr., J. R. Mecikalski, and C. P. Jewett, 2012: An enhanced geostationary satellite-based convective initiation algorithm for 0–2-h nowcasting with object tracking. *J. Appl. Meteor. Climatol.*, **51**, 1931–1949, doi:10.1175/JAMC-D-11-0246.1.
- Walther, A., and A. K. Heidinger, 2012: Implementation of the daytime cloud optical and microphysical properties algorithm (DCOMP) in PATMOS-x. *J. Appl. Meteor. Climatol.*, **51**, 1371–1390, doi:10.1175/JAMC-D-11-0108.1.
- Wang, P. K., 2007: The thermodynamic structure atop a penetrating convective thunderstorm. *Atmos. Res.*, **83**, 254–262, doi:10.1016/j.atmosres.2005.08.010.
- Wilson, J. W., and W. E. Schreiber, 1986: Initiation of convective storms by radar-observed boundary-layer convergent lines. *Mon. Wea. Rev.*, **114**, 2516–2536, doi:10.1175/1520-0493(1986)114<2516:IOCSAR>2.0.CO;2.
- , and C. K. Mueller, 1993: Nowcasts of thunderstorm initiation and evolution. *Wea. Forecasting*, **8**, 113–131, doi:10.1175/1520-0434(1993)008<0113:NOTIAE>2.0.CO;2.
- , G. B. Foote, N. A. Crook, J. C. Fankhauser, C. G. Wade, J. D. Tuttle, C. K. Mueller, and S. K. Kruger, 1992: The role of boundary-layer convergence zones and horizontal rolls in the initiation of thunderstorms: A case study. *Mon. Wea. Rev.*, **120**, 1785–1815, doi:10.1175/1520-0493(1992)120<1785:TROBLC>2.0.CO;2.

NEW FROM AMS BOOKS!

A Scientific Peak: How Boulder Became a World Center for Space and Atmospheric Science

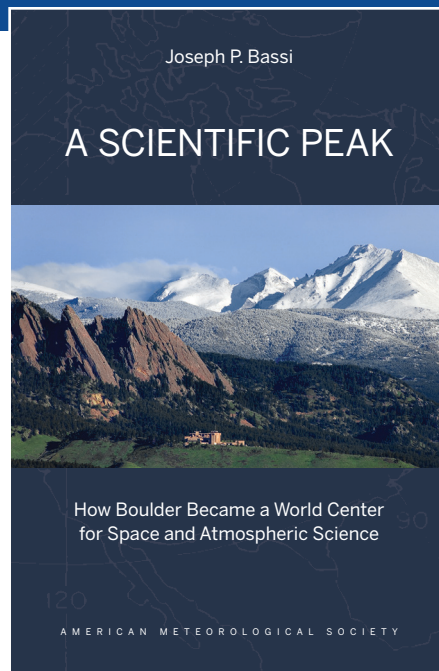
Joseph P. Bassi

Once a Wild West city tucked between the Rocky Mountains and the Great Plains, Boulder is now home to some of the biggest names in science, including NCAR, NOAA, and NIST.

Why did big science come to Boulder? How did Boulder become the research mecca it is today?

A Scientific Peak is a fascinating history that introduces us to a wide variety of characters, such as Walter Orr Roberts, and the serendipitous brew of politics, passion, and sheer luck that, during the post-WWII and Cold War eras, transformed this “scientific Siberia” into one of America’s smartest cities.

© 2015, 264 pages, paperback
 print ISBN: 978-1-935704-85-0 eISBN: 978-1-940033-89-1
 List price: \$35 AMS Member price: \$25



AMS BOOKS

RESEARCH APPLICATIONS HISTORY

> bookstore.ametsoc.org